Contact points open wide band gaps in all two-dimensional Bravais lattices

David Röhlig [1,2,3,*] Ralf Zichner [4,5] Thomas Blaudeck [3,5] Angela Thränhardt,[2] and Vincent Laude [1,†]

[1] *Université Marie et Louis Pasteur, CNRS, Institut FEMTO-ST, 15B avenue des Montboucons, 25030 Besançon, France*

[2] *Technische Universität Chemnitz, Institute of Physics, Reichenhainer Straße 70, 09126 Chemnitz, Germany*

[3] *Research Center for Materials, Architectures and Integration of Nanomembranes (MAIN), Chemnitz University of Technology, Rosenbergstraße 6, 09126 Chemnitz, Germany*

[4] *Faculty of Electrical Engineering and Information Technology, Chemnitz University of Technology, Reichenhainer Str. 70, 09126 Chemnitz, Germany*

[5] *Fraunhofer Institute for Electronic Nano Systems (ENAS), Technologie-Campus 3, 09126 Chemnitz, Germany*

(Received 5 November 2025; revised 20 January 2026; accepted 2 April 2026; published 30 April 2026)

The propagation of waves in crystals is known to be strongly affected by the choice and the spatial distribution of inclusions in a matrix. We argue herewith that in-contact, impermeable inclusions lead to extremely wide band gaps for all 2D Bravais lattices. Contact points entail constrictions that efficiently slow wave propagation and lead to strongly flattened bands. A numerical demonstration is provided for a generic Helmholtz equation that is applicable to electromagnetic, acoustic, elastic, or water waves alike. Experiments conducted on square and hexagonal photonic crystals composed of touching copper tubes reveal that waves of certain radio frequencies quite remarkably traverse the minute gaps within the metallic framework, thereby confirming the theoretical predictions, including the presence of deeply subwavelength Bragg band gaps.

DOI: 10.1103/9ql7-t9rh

I. INTRODUCTION

Periodic media act as barriers to waves of certain frequencies. This phenomenon has been verified across a wide portfolio of wave types—beginning with electron waves in atomic lattices and extending to light [1], elastic waves [2] such as sound [3], seismic [4], thermal [5], or water waves [6], spin waves [7], and beyond. When departing from the atomic scale, such structures are commonly referred to as artificial crystals [8]. The frequency intervals, or band gaps, within which waves cannot propagate owing to the exclusive presence of evanescent modes, may arise from different mechanisms [9]: One such is Bragg reflection, originally discovered for x-ray radiation [10]; it stems purely from periodicity, giving rise to Bragg gaps that open at high-symmetry points of the reciprocal lattice. A second mechanism involves local resonances internal to the crystal [11]—a phenomenon that has attracted considerable scholarly attention, as the position of the frequency gap is not governed solely by periodicity.

A central objective, naturally, is the pursuit of the widest possible gaps. One might assume that the question of maximizing gap width has long been settled—it has, after all, accompanied the study of artificial crystals since its very beginnings. More recently, optimization algorithms and deep-learning techniques have been devised explicitly for this purpose [12–15]. Considerable progress has indeed been made: It is now common knowledge that the extent of a band gap is determined by several factors, broadly classifiable according to material and geometric aspects. On the material side, high parameter contrast is recognized to promote large gaps [7,16–18]; impermeable inclusions naturally maximize this contrast. If a material exhibits resonance with respect to the wave type considered, the degree of coupling between the lattice constituents becomes decisive for the resulting gap width [9]. By combining this mechanism with Bragg scattering—for instance, by coupling masses through ligament walls in phononic crystals—an optimized widening of the band gap can be achieved [19,20].

From a geometric perspective, lattice symmetry obviously plays a role in Bragg crystals; in addition, the ratio between matrix and inclusion—the so-called filling fraction—serves as a vital tuning parameter, as increasing inclusion size typically enlarges the gap [21]. In a few articles, it has been noted that close packing of solid scatterers may promote the formation of wide band gaps [22–26]. However, this phenomenon has not yet been subjected to systematic investigation, particularly with regard to the role of the contact regions between the inclusions. Recently, we have experimentally presented emergence of wide band gaps in sonic crystals with touching candles. The findings were accompanied by the appearance of flat-band characteristics in the band structures [27]; owing to the intrinsically low group velocities, flat bands have attracted considerable scholarly interest within the field of artificial crystals [1,28]. The essence of the findings may be stated succinctly: the largest band gaps occur when impermeable

*Contact author: david.rohlig@femto-st.fr

†Contact author: vincent.laude@femto-st.fr

inclusions are in punctual contact—theoretically, infinitesimally so. The underlying effect is evidenced to be fundamental, and yet, remarkably, it had thus far evaded systematic recognition. Two plausible reasons explain this situation. The first originates from numerical methodology: traditional Fourier-based approaches—notably the plane-wave expansion method—fail to accurately capture small contact regions due to Gibbs oscillations caused by discontinuities of material constants [29,30]. Likewise, multiple-scattering techniques are expected to face challenges when attempting to incorporate overlapping conditions [31]. The second relates to fabrication constraints: Contact points emerge in both two- and three-dimensional crystals. In the latter case, contact points may have been employed unintentionally—as they are likely to arise naturally when inclusions are stacked upon one another [32]. For 2D systems, however, they are often excluded *a priori*; for example, in structures produced by drilling holes into a solid medium, a finite separation between inclusions is required to ensure mechanical stability [21].

In this article, we argue that the proposed criterion of contact points possesses universal validity and applies to crystals in general. Contacts create constrictions that canalize and efficiently slow wave propagation, leading to flat bands and hence wide band gaps. Experiments at radio frequencies with a 2D photonic crystal of copper tubes sustain this conclusion.

II. BAND STRUCTURE CALCULATIONS

As noted, several mechanisms can give rise to wide band gaps—yet contact points, as we intend to emphasize, must be regarded as one of the decisive factors. To discern their influence most clearly, it is advantageous to consider materials exhibiting a pronounced contrast in parameters. The idealized case is provided by inclusions that are impermeable to the considered wave—thereby deliberately excluding resonances, which, though capable of substantially enlarging band gaps, could obscure the specific effect under investigation. The assumption of impermeable inclusions considerably simplifies the mathematical treatment: since wave fields cannot penetrate them, there is no need to account for their interior within the computational domain. The inclusion is thus represented solely by a boundary condition, and consequently, only a single material region remains to be treated in the calculations. We therefore consider the Helmholtz equation in the form

$$\triangle\psi(\boldsymbol{r}) = -\frac{\omega^2}{c^2}\psi(\boldsymbol{r}), \tag{1}$$

where ω denotes the angular frequency, c the propagation speed, and ψ represents the wave field. To determine the band structure of two-dimensional crystals, we employed the finite element method (FEM), which requires a variational formulation including a generic test function $\tilde{\psi}$. By introducing Bloch solutions $\psi(\boldsymbol{r},t) = \psi(\boldsymbol{r})\exp(i\omega t - i\boldsymbol{k}\cdot\boldsymbol{r})$ for both the field and the test function, we can derive the following expression:

$$\frac{\omega^2}{c^2}\int_\Omega \tilde{\psi}\,\psi\,\mathrm{d}\boldsymbol{r} = \int_\Omega (\nabla + i\boldsymbol{k})\tilde{\psi}\cdot(\nabla - i\boldsymbol{k})\psi\,\mathrm{d}\boldsymbol{r} - \int_{\partial\Omega}\tilde{\psi}(\nabla - i\boldsymbol{k})\psi\cdot\boldsymbol{n}\,\mathrm{ds}, \quad \forall\tilde{\psi}. \tag{2}$$

The functions $\tilde{\psi}$ and ψ represent the periodic parts of the Bloch waves. The first two integrals are defined over the unit cell domain Ω, which consists of a single material. The last term involves integrals along internal boundaries $\partial\Omega$, incorporating the normal vectors $\boldsymbol{n}$. For impermeable inclusions, only two boundary conditions are admissible—Neumann and Dirichlet. Along the external boundaries, periodic boundary conditions are imposed, resulting in the cancellation of the corresponding boundary integrals.

To demonstrate that contact points constitute a powerful mechanism for band flattening and for the emergence of complete frequency gaps regardless of lattice symmetry, we computed band structures corresponding to all possible lattice types, for circular inclusions preserving the symmetry of the five 2D Bravais lattices. The most general case is the oblique lattice, characterized by the lowest degree of symmetry. It can be described by two basis vectors, $\boldsymbol{a}_1$ and $\boldsymbol{a}_2$. By varying their magnitudes and the angle between them, symmetry can be systematically increased. The unit cells of the five lattices that were used for band structure calculations are depicted in Fig. 1. The paths in k space were traced along the respective high-symmetry points—whose number increases as symmetry decreases—following the conventions established by Setyawan and Curtarolo [33]; they are depicted in Fig. 7. The resulting calculations, displayed in Figs. 2(a)–2(e), were performed using software FreeFem ++ [34]. We employed a triangular mesh of P2 elements with a resolution of 30 points per lattice constant a_1 along the boundaries. It was constructed such that the intersection of two inclusions occurs precisely at a single mesh point; this is illustrated in Fig. 2(f) for one representative contact point. Each band structure was computed for both Neumann and Dirichlet boundary conditions (BCs). For the latter, there is a zero-frequency band gap. Unlike for Neumann BC, bands for the Dirichlet BC do not originate from zero at the Γ point; rather, they emerge at cut off frequencies, thereby excluding low-frequency modes. Such behavior has previously been observed in platonic phononic [35] or metallic photonic crystals [36].

Do contact points influence band gaps regardless of the underlying periodic arrangement? Remarkably, even for lattices of low symmetry, the band structures in Figs. 2(a)–2(c) exhibit complete gaps for both types of boundary conditions. The fact that the oblique lattice, despite its minimal symmetry, produces full band gaps underscores that the flattening effect induced by contact points does not rely on high-symmetry conditions. The rectangular lattice, in particular, elucidates the underlying mechanism: the path Γ to X extends along the direction in which the impermeable inclusions remain separated—some space persists between them. In contrast, the path from Γ to Y corresponds to the direction where circles forming Bragg planes are in contact; consequently, the band gaps widen substantially around Y compared to X. For the rhombic lattice, analogous effects emerge, aside from specific band crossings arising from the intrinsic lattice symmetry, thereby confirming the general trend. We have thus established that contact points foster gap formation even in lattices of reduced symmetry. It is, therefore, reasonable to expect even broader gaps in square and hexagonal lattices, which both satisfy $a_1 = a_2$ and include a fourfold and sixfold rotational symmetry,

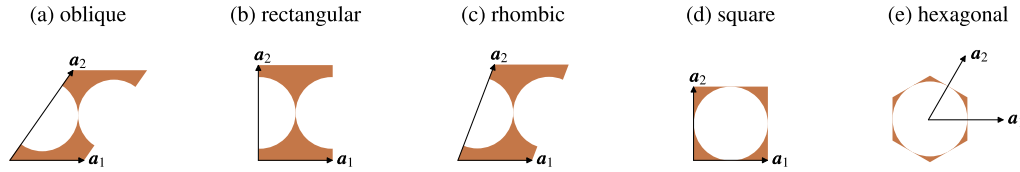

FIG. 1. The five Bravais lattices of 2D crystals. Primitive unit cells are shown for the case of impermeable, in-contact, circular inclusions. For lattices (a)–(d), the primitive unit cells were used; for (e), the Wigner-Seitz cell containing a closed inclusion was defined. The corresponding Brillouin zones are presented in Fig. 7. Per unit cell, there are one contact point for oblique, rectangular, and rhombic lattices, two contact points for the square lattice, and three contact points for the hexagonal lattice.

respectively. Indeed, the results disclose exceptionally wide gaps for the square lattice—and still more pronounced ones for the hexagonal configuration; we thus find ourselves within the regime of ideal conditions for the emergence of extensive band gaps. Notably, these gaps lie within the deeply subwavelength regime: for instance, in the square lattice, the maximum of the first band corresponds to a wavelength ten times the lattice constant $a-$, a phenomenon atypical for a Bragg gap and of clear relevance for metamaterial applications [37]. Without the points of contact, and the constriction they define, such behavior would remain unattainable.

How do Bloch waves behave precisely at contact points? An indication can be obtained from the Poynting vector $\boldsymbol{S}$. From the eigenvectors at the X point of the square lattice and at the M point of the hexagonal lattice, the corresponding Poynting vectors were computed for the first three bands,

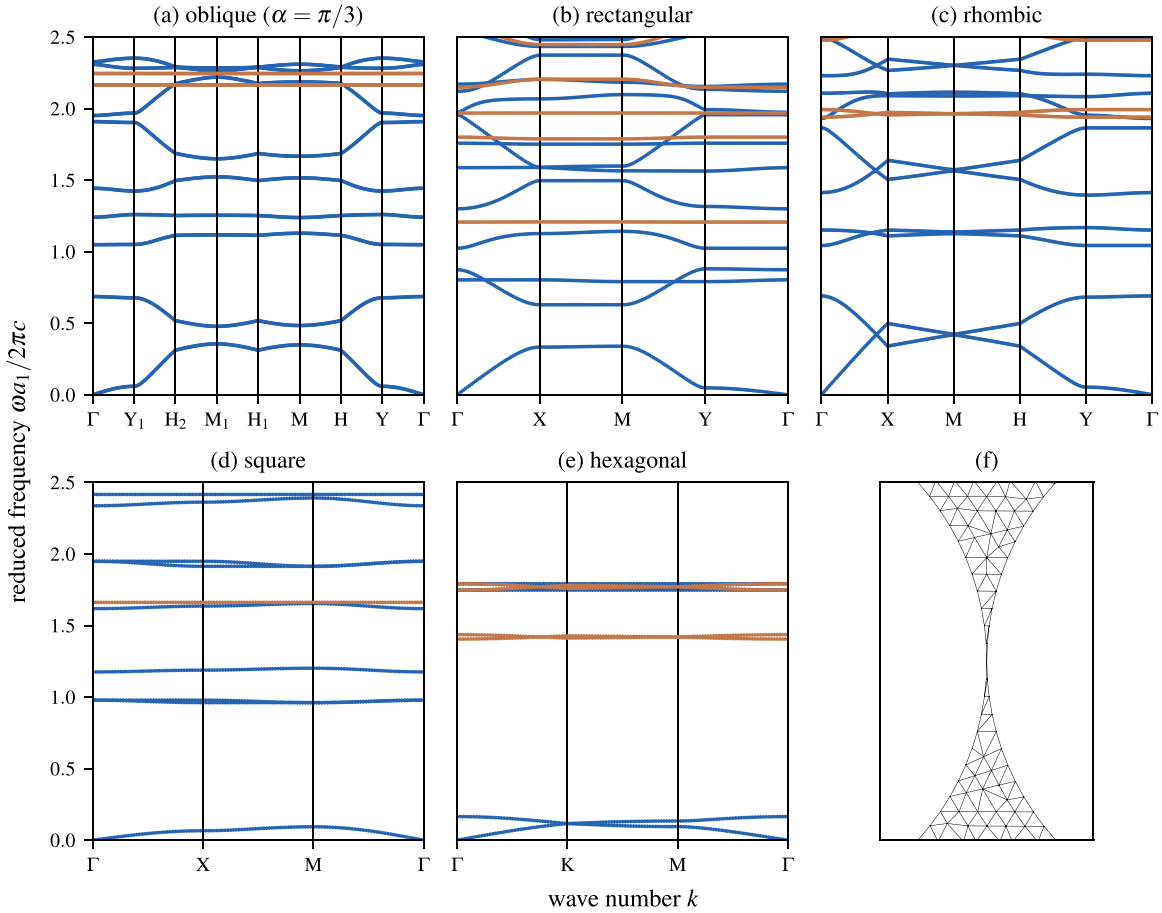

FIG. 2. Band gaps of 2D crystals of in-contact, impermeable inclusions. Band structures (a)–(e) of the five two-dimensional Bravais lattices, consisting of inclusions with a diameter that equals the lattice constant a_1 are shown for both Neumann (in blue) and Dirichlet conditions (in brown), plotted along the paths connecting their respective symmetry points that are depicted in Fig. 7. Where the two lattice constants are not equal by definition (d), (e), the scaling between the lattice constants was set to $a_2 = 1.2\,a_1$ for (a)–(c). The contact points give rise to the emergence of gigantic complete band gaps in the high-symmetry lattices (d), (e), and to gaps of considerable width in the lower-symmetry configurations (a)–(c). Panel (f) depicts the finite element mesh resolved with 30 points per lattice constant a_1 at the boundaries—around a contact point between two impermeable inclusions.

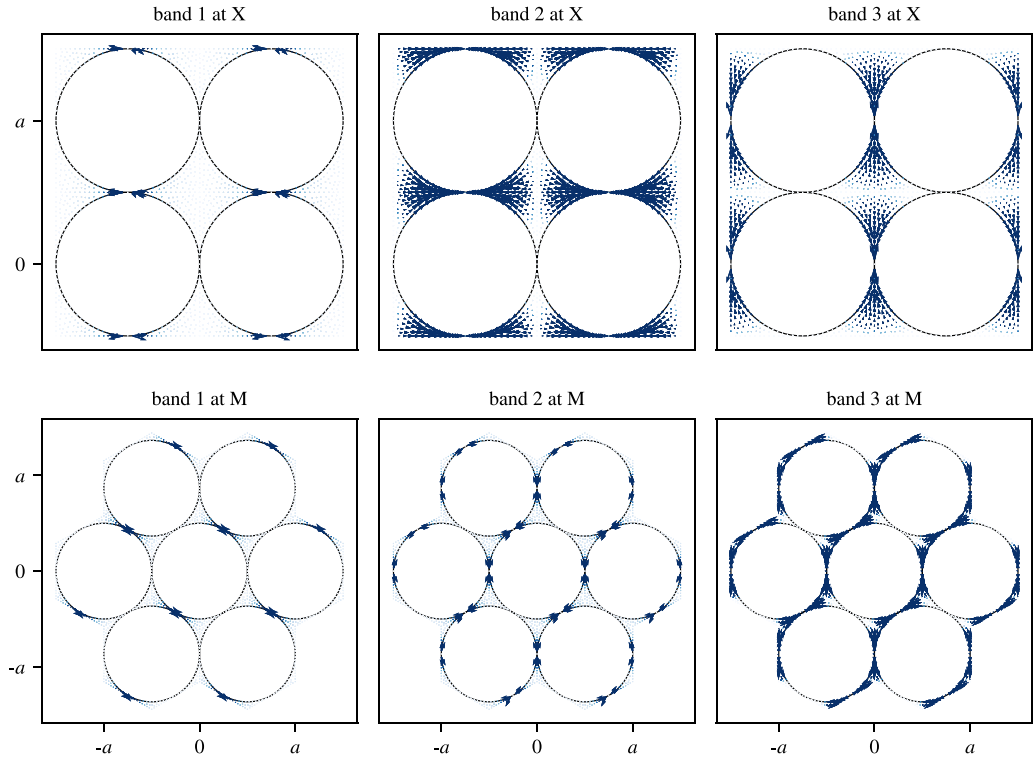

FIG. 3. The spatial distribution of the Poynting vector—derived from the eigenvectors obtained in the calculation shown in Figs. 2(d) and 2(e). The unit cell was periodically replicated according to the symmetries of the square and hexagonal lattices. The resulting patterns are displayed for the first three bands at the high-symmetry points X and M corresponding to the measurement directions chosen for the experiments.

respectively. For TM waves, they were obtained according to

$$\boldsymbol{S} = \mathrm{Re}\left[\frac{1}{2i\omega c^2}\begin{pmatrix}\partial_x H_z^2\\ \partial_y H_z^2\\ 0\end{pmatrix}\right]. \tag{3}$$

Figure 3 illustrates the spatial distribution of the Poynting vector within the unit cell. The results reveal a clear and consistent tendency: the energy density concentrates more strongly at the contact points than within the cavities—regions where, in the presence of resonances, localization would otherwise be expected. As waves are compelled to traverse bottlenecklike constrictions, their celerity is markedly reduced—that manifests itself as the emergence of flat bands in the band structure.

III. TRANSITION FROM SEPARATED TO TOUCHING INCLUSIONS

To elucidate the transition from the well-known case of nontouching inclusions to the regime of contact points, we depict the band edges surrounding the first band gap as a function of the inclusion diameter in Fig. 4—shown here exemplarily for the square lattice. Upon the emergence of a contact point, the bands progressively flatten, and a pronounced as well as abrupt opening of the band gap becomes clearly apparent. In addition, we investigate the dependence of the band edges on the mesh resolution. It turns out that 30 points per lattice constant, defined along the boundaries, are sufficient to ensure convergence in almost all cases. An exception arises for the lower band edge in for exact touching, where convergence is noticeably slower. As a consequence, the large band gaps reported here are, at the chosen resolution, in fact underestimated. In practical terms, however, this limitation remains well below the fabrication tolerances of the experimental structures. For a converged lower band, the width of the first gap, normalized to the average of the edge frequencies, reaches 1.88 for the square lattice and 1.86 for

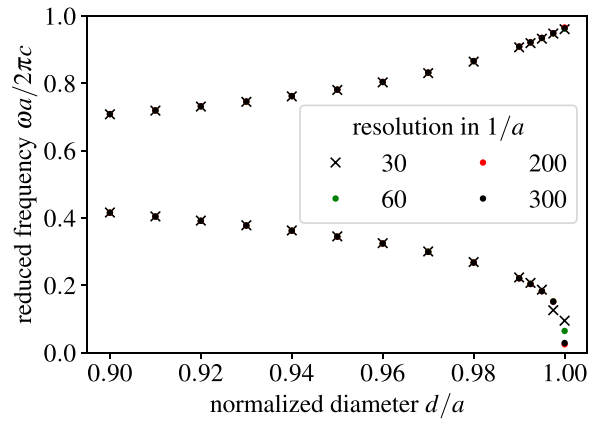

FIG. 4. Evolution of the band-edge frequencies for the square lattice as a function of the inclusion diameter d, normalized to the lattice constant a. The mesh resolution is indicated for values between 30 to 300 nodes per lattice constant along the boundaries.

the hexagonal lattice. In the hexagonal case, the first band gap is located between the second and third band.

IV. EXPERIMENTAL VALIDATION

To translate numerical results into practice, we provide an experimental demonstration. Our objective is to investigate the effect of contact points within a material system that remains readily accessible. Electromagnetic waves were selected as the platform of investigation—in this context, the periodically structured medium is referred to as a photonic crystal. To emulate impermeable inclusions, a highly conductive metal—such as copper—constitutes an ideal choice in the regime of long-wavelength electromagnetic waves. It may be modeled as a so-called perfect electric conductor (PEC). At its boundary, characterized by the normal vector $\boldsymbol{n}$, the tangential electric field vanishes—formally expressed as $\boldsymbol{E} \times \boldsymbol{n} = 0$. Under that assumption, geometric features on length scales smaller than the skin depth are implicitly ignored; consequently, the mathematically singular nature of the contact point does not carry practical significance in either computation or experiment.

In addition to the PEC, air is chosen as the surrounding medium. Within reasonable accuracy, its relative permittivity and permeability can both be approximated as unity. Starting from Maxwell's equations, the assumption of time-harmonic fields gives rise to an eigenvalue problem—identical in form to Eq. (1). The two boundary conditions imposed in this article to ensure impermeability admit a direct physical correspondence to the two fundamental polarizations of light in a two-dimensional photonic crystal: TE modes, where the electric field is perpendicular to the plane of periodicity ($\psi = E_z$) and TM modes, where it is the magnetic field ($\psi = H_z$). The two boundary conditions imposed in the weak formulation Eq. (2) correspond directly to these modes. For TE modes, the PEC condition resembles the Dirichlet condition with $\psi = E_z = 0$. For TM modes, applying the PEC condition to Ampère's law yields $0 = \boldsymbol{n} \cdot \nabla H_z -$, a relation that represents a Neumann boundary condition. More details can be found elsewhere [38].

To compare theoretical predictions with experimental observations, we conducted transmission measurements in an anechoic chamber. Figure 5 (see also Fig. 8 in Appendix B) illustrates the experimental setup, tailored for long-wavelength electromagnetic radiation in the gigahertz regime. The chosen square and hexagonal lattice structures consist of copper tubes whose diameter equals the lattice constant a_1, implying that they are in mutual contact. Each tube has a diameter of 42 mm, a wall thickness of 1.2 mm, and a height of 20 cm. Tubes are arranged in a 7×7 array embedded in air. This size suffices to resolve the band gaps; additional rows along the measurement direction merely suppress evanescent contributions and deepen the transmission minima. To ensure a straight contact line of optimal mechanical contact, they were inserted into premilled wooden base plates. The experimental setup includes a vector network analyzer (model: Rohde & Schwarz ZVL6) and two horn antennas (model: Schwarzbeck BBHA 9120 B), both connected via coaxial cables and mounted on tripods at the height of the copper structure, each positioned three lattice constants a_1 away from the outermost

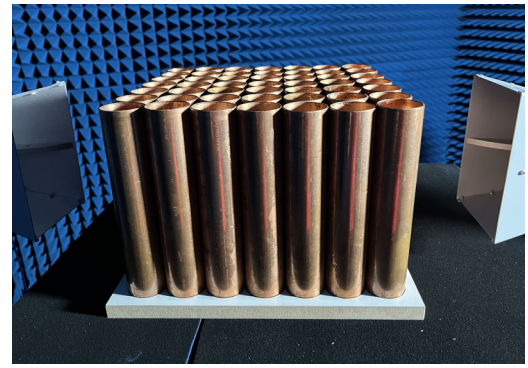

FIG. 5. Photograph of a two-dimensional photonic crystal consisting of a 7×7 array of copper tubes arranged in a square lattice—positioned within an anechoic chamber for transmission measurements using horn antennas.

row, and aligned face to face. Using the network analyzer, we recorded the scattering parameters S corresponding to the $\Gamma-$X direction for the square lattice and the $\Gamma-$M direction for the hexagonal lattice in reciprocal space. Each data point represents an average over 50 individual measurements taken from sensor one to sensor two (S_{21}) and vice versa (S_{12}); the final transmission curve is their mean. Additionally, a reference measurement S^0 was conducted without the

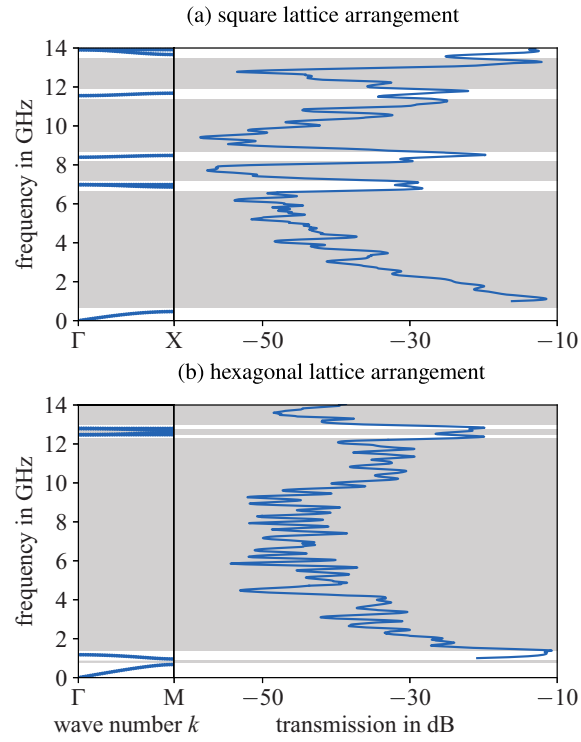

FIG. 6. The band structures of both the square and hexagonal lattices—computed via FEM for the unit cells depicted in Figs. 1(d) and 1(e)—are juxtaposed with the corresponding transmission measurements obtained from the copper-tube configuration: (a) along the $\Gamma-$X direction for the square (see Fig. 5) and (b) along $\Gamma-$M for the hexagonal arrangement (see Fig. 8).

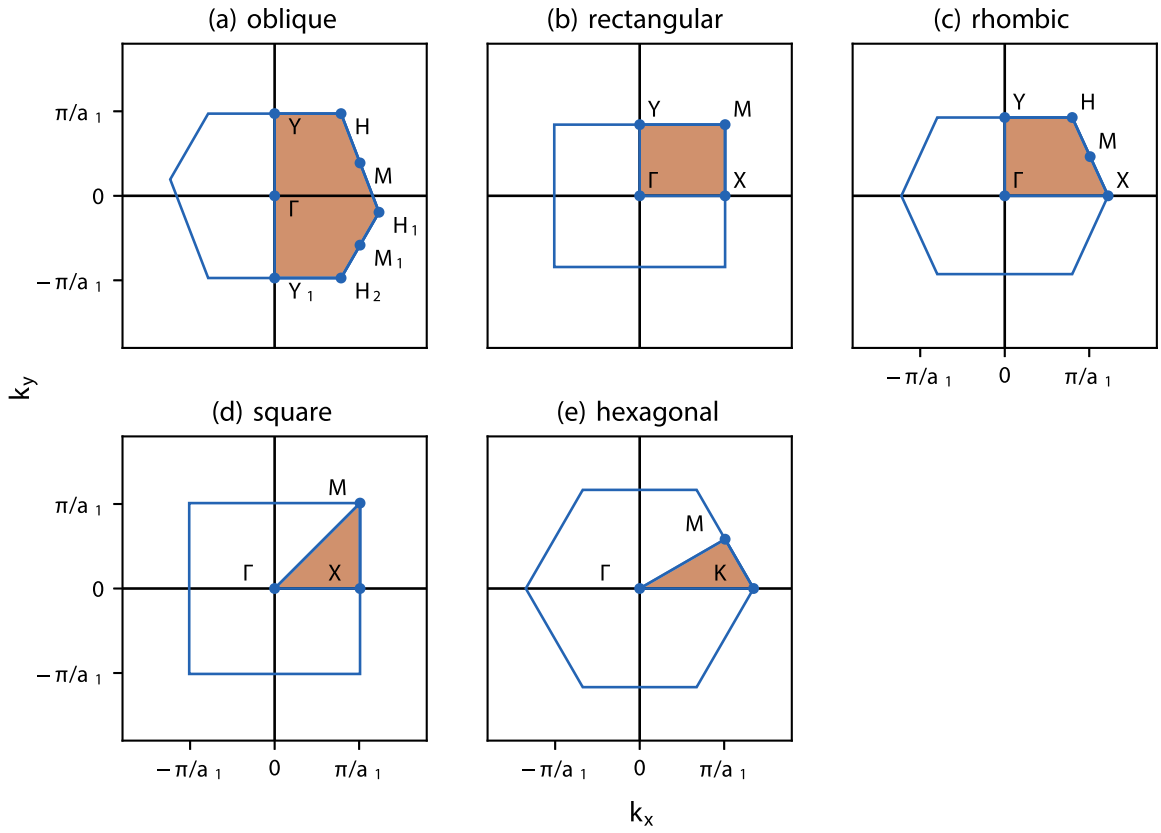

FIG. 7. The Brillouin zones of the five two-dimensional Bravais lattices are shown according to established definitions [33] and the parameter values used to compute the band structures in Fig. 2 of the main text. For each lattice, the irreducible Brillouin zone is highlighted.

structure placed between the antennas, serving as the baseline for normalization.

The results for the square and hexagonal lattice configurations of copper tubes are presented in Fig. 6. Overall, the experimental data for TM modes exhibit pronounced frequency-dependent variations in transmission, in excellent agreement with the theoretically predicted band structures. While the flat bands are clearly emphasized by transmission maxima, the giant Bragg gaps—opening at the high-symmetry points—manifest themselves as distinct spectral dips in the two transmission curves. Along the Γ−M direction for the hexagonal lattice, two band pairs become discernible within the chosen frequency range. Notably, even for the narrow gaps between bands one and two, as well as between bands three and four, the measurements display a clear correspondence, evidenced by a marked decrease in transmission. As explained in Ref. [39], this single curve suffices to establish the completeness of the gap. Due to the existence of contact points, we testify a highly optimized system for achieving significant and broadband wave attenuation.

V. SUMMARY

Through a combination of numerical analysis and experimental validation, we have demonstrated the existence of a fundamental geometric criterion for achieving maximal band-gap sizes in crystals. Contact points prove exceptionally potent in this regard: they form constrictions that concentrate states within narrow frequency bands with low group velocities, thereby giving rise to exceptionally large complete gaps. This effect is most pronounced for inclusions that are impermeable to waves. Crucially, this phenomenon is not restrictetd to particular lattice symmetries; it extends across all Bravais lattices—including those of low symmetry, such as the oblique class. When the degree of symmetry increases, however, these effects become especially pronounced, giving rise to deeply subwavelength gaps for the square and hexagonal lattice—notably, not of the locally resonant, but of the Bragg type. Experimental results corroborate that these enormous gaps are not mere numerical artifacts but can, in fact, be realized with relative ease in practice. It would be interesting to extend the present analysis to vector waves—beyond the scalar Helmholtz equation considered herewith—and to investigate configurations involving touching impermeable inclusions by introducing periodicity in the third dimension. We anticipate that these findings will inform and reorient future research on artificial crystals—ranging from engineering thermal conductivity by acoustic phonons to designing systems for seismic or acoustic noise protection, as well as for applications based on slow light. Beyond their immediate implications, our findings invite a renewed reflection on the mechanisms of band structure formation, which is expected to also enhance the overall effectiveness of metamaterials.

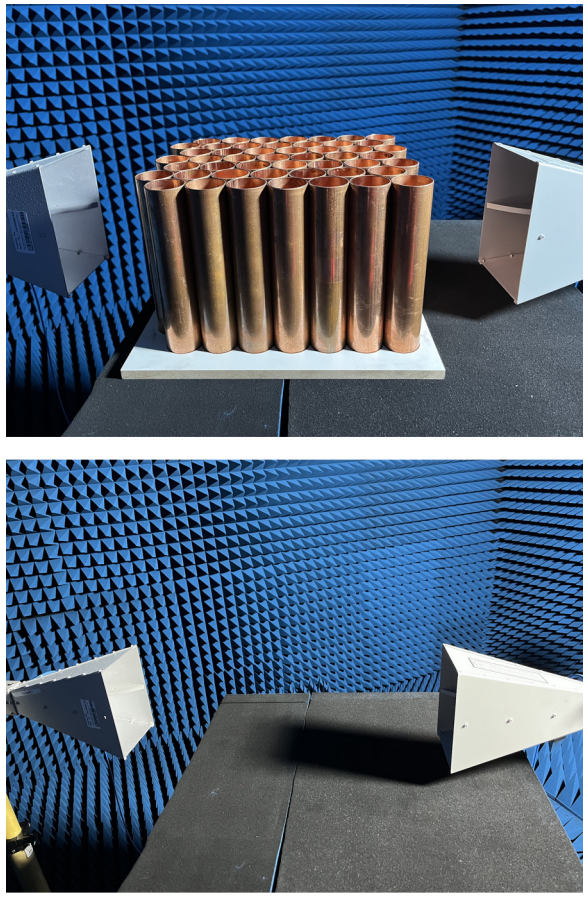

FIG. 8. Photograph of a two-dimensional photonic crystal composed of a 7×7 array of copper tubes arranged in a hexagonal configuration (top). Measurements were performed along the $\Gamma-\mathrm{M}$ direction in k space within an anechoic chamber, employing horn antennas for transmission analysis. For the reference measurement, the structure was removed (bottom).

ACKNOWLEDGMENTS

We gratefully acknowledge Ralf Jacob for confectioning the copper tubes as well as Andreas Nendel (both TUC Technical Services) and Fabian Nendel (Research Center MERGE, Chemnitz University of Technology) for the fabrication of the wooden base plate—both components were employed in the experiments. This work was supported by the EIPHI Graduate School [Grant No. ANR-17-EURE-0002] and the TUCculture2025 initiative of Chemnitz University of Technology.

DATA AVAILABILITY

The data that support the findings of this article are not publicly available upon publication because it is not technically feasible and/or the cost of preparing, depositing, and hosting the data would be prohibitive within the terms of this research project. The data are available from the authors upon reasonable request.

APPENDIX A: BRILLOUIN ZONES FOR 2D CRYSTALS

In the main text, we have demonstrated that contact points between touching impermeable inclusions flatten bands and open gaps across all possible lattice symmetries. Band structures were presented for the five two-dimensional Bravais lattices; the corresponding Brillouin zones, including their symmetry points, are shown in Fig. 7, defined consistently with the geometry parameters used in the calculations.

APPENDIX B: EXPERIMENTAL SETUP

The transmission experiments were conducted in an anechoic chamber. Two distinct measurements were performed: one with the copper structure in place, and one in the absence of the structure. Figure 8 illustrates both the setup for the reference measurement S^0 and the measurement of the hexagonal arrangement of copper tubes along the direction corresponding to the $\Gamma-\mathrm{M}$ path in k space.

The noise observed in the data presented in Fig. 4 of the main text can be traced to two primary sources. First, the intrinsic noise limit of the vector network analyzer, which becomes particularly evident within the band-gap range; and second, minor discrepancies between the two horn antennas, most pronounced in regions of high transmission (within the bands) and under conditions of elevated measurement resolution.

The frequency-dependent characteristics of the antennas—including S_{11}, impedance, voltage standing wave ratio (VSWR), and actual antenna gain—never align perfectly, even for nominally identical models. Consequently, the seemingly noisy S_{21} measurement accurately reflects the genuine, frequency-specific transmission behavior at high resolution. To mitigate these effects, data smoothing was applied using a Savitzky-Golay filter with fourth-order polynomials and a window size of 80 coefficients.

[1] C. T. Chan, Essay: Photonic crystals as a platform to explore new physics, Phys. Rev. Lett. **135**, 080001 (2025).

[2] M. S. Kushwaha, P. Halevi, L. Dobrzynski, and B. Djafari-Rouhani, Acoustic band structure of periodic elastic composites, Phys. Rev. Lett. **71**, 2022 (1993).

[3] R. Martínez-Sala, J. Sancho, J. V. Sánchez, V. Gómez, J. Llinares, and F. Meseguer, Sound attenuation by sculpture, Nature (London) **378**, 241 (1995).

[4] S. Brûlé, E. H. Javelaud, S. Enoch, and S. Guenneau, Experiments on seismic metamaterials: Molding surface waves, Phys. Rev. Lett. **112**, 133901 (2014).

[5] M. Nomura, R. Anufriev, Z. Zhang, J. Maire, Y. Guo, R. Yanagisawa, and S. Volz, Review of thermal transport in phononic crystals, Mater. Today Phys. **22**, 100613 (2022).

[6] S. Zhu, X. Zhao, L. Han, J. Zi, X. Hu, and H. Chen, Controlling water waves with artificial structures, Nat. Rev. Phys. **6**, 231 (2024).

[7] S. Tacchi, G. Duerr, J. W. Klos, M. Madami, S. Neusser, G. Gubbiotti, G. Carlotti, M. Krawczyk, and D. Grundler, Forbidden band gaps in the spin-wave spectrum of a two-dimensional bicomponent magnonic crystal, Phys. Rev. Lett. **109**, 137202 (2012).

[8] A. V. Chumak, V. S. Tiberkevich, A. D. Karenowska, A. A. Serga, J. F. Gregg, A. N. Slavin, and B. Hillebrands, All-linear time reversal by a dynamic artificial crystal, Nat. Commun. **1**, 141 (2010).

[9] V. Laude, Local resonance and Fano resonance, *Phononic Crystals* (De Gruyter, Berlin, München, Boston, 2015), Chap. 10.1, pp. 303–327.

[10] W. H. Bragg, The reflection of x-rays by crystals. (II.), Proc. A **89**, 246 (1913).

[11] Z. Liu, X. Zhang, Y. Mao, Y. Y. Zhu, Z. Yang, C. T. Chan, and P. Sheng, Locally resonant sonic materials, Science **289**, 1734 (2000).

[12] R. T. Bonnecaze and J. Søndergaard Jensen, Systematic design of phononic band–gap materials and structures by topology optimization, Philos. Trans. R. Soc. Lond. Ser. A **361**, 1001 (2003).

[13] J. Jensen and O. Sigmund, Topology optimization for nano-photonics, Laser Photon. Rev. **5**, 308 (2011).

[14] W. Li, F. Meng, Y. Chen, Y. f. Li, and X. Huang, Topology optimization of photonic and phononic crystals and metamaterials: A review, Adv. Theor. Simul. **2**, 1900017 (2019).

[15] J. Li, M. Qian, J. Yin, W. Lin, Z. Zhang, and S. Liu, Topology design of soft phononic crystals for tunable band gaps: A deep learning approach, Materials **18**, 377 (2025).

[16] J. D. Joannopoulos, S. G. Johnson, J. N. Winn, and R. D. Meade, Atlas of band gaps, *Photonic Crystals* (Princeton University Press, USA, 2008), pp. 242–251.

[17] Z.-f. Liu, B. Wu, and C. fu He, Band-gap optimization of two-dimensional phononic crystals based on genetic algorithm and fpwe, Waves Random Complex Medium **24**, 286 (2014).

[18] G. Morales-Morales and J. Manzanares-Martinez, Enlargement of band gaps on thermal wave crystals by using heterostructures, Results Phys. **42**, 106019 (2022).

[19] Z. Jia, Y. Chen, H. Yang, and L. Wang, Designing phononic crystals with wide and robust band gaps, Phys. Rev. Appl. **9**, 044021 (2018).

[20] J. A. Iglesias Martínez, J. Moughames, G. Ulliac, M. Kadic, and V. Laude, Three-dimensional phononic crystal with ultra-wide bandgap at megahertz frequencies, Appl. Phys. Lett. **118**, 063507 (2021).

[21] C. M. Reinke, M. F. Su, I. R. H. Olsson, and I. El-Kady, Realization of optimal bandgaps in solid-solid, solid-air, and hybrid solid-air-solid phononic crystal slabs, Appl. Phys. Lett. **98**, 061912 (2011).

[22] M. S. Kushwaha, Stop-bands for periodic metallic rods: Sculptures that can filter the noise, Appl. Phys. Lett. **70**, 3218 (1997).

[23] D. Caballero, J. Sánchez-Dehesa, C. Rubio, R. Mártinez-Sala, J. V. Sánchez-Pérez, F. Meseguer, and J. Llinares, Large two-dimensional sonic band gaps, Phys. Rev. E **60**, R6316 (1999).

[24] D. Röhlig, E. Kuhn, F. Teichert, A. Thränhardt, and T. Blaudeck, Function phononic crystals, Europhys. Lett. **145**, 26001 (2024).

[25] P. Lambin, A. Khelif, J. O. Vasseur, L. Dobrzynski, and B. Djafari-Rouhani, Stopping of acoustic waves by sonic polymer-fluid composites, Phys. Rev. E **63**, 066605 (2001).

[26] Y. Liang, G. Yun, H. Yang, N. Bai, and Y. Cao, Dirac points and flat bands in two-dimensional magnonic crystals with honeycomb–kagome structure, AIP Adv. **14**, 035242 (2024).

[27] D. Röhlig, A. Thränhardt, V. Laude, and T. Blaudeck, Giant band gaps in a phononic crystal with touching solid inclusions, Phys. Rev. Appl. **23**, 054055 (2025).

[28] L. Tang, D. Song, S. Xia, S. Xia, J. Ma, W. Yan, Y. Hu, J. Xu, D. Leykam, and Z. Chen, Photonic flat-band lattices and unconventional light localization, Nanophoton. **9**, 1161 (2020).

[29] L. Li, Use of fourier series in the analysis of discontinuous periodic structures, J. Opt. Soc. Am. A **13**, 1870 (1996).

[30] H. S. Sözüer, J. W. Haus, and R. Inguva, Photonic bands: Convergence problems with the plane-wave method, Phys. Rev. B **45**, 13962 (1992).

[31] R. Sainidou, N. Stefanou, I. Psarobas, and A. Modinos, A layer-multiple-scattering method for phononic crystals and heterostructures of such, Comput. Phys. Commun. **166**, 197 (2005).

[32] J. D. Joannopoulos, S. G. Johnson, J. N. Winn, and R. D. Meade, Three-dimensional photonic crystals, *Photonic Crystals* (Princeton University Press, USA, 2008), Chap. 6, pp. 94–121.

[33] W. Setyawan and S. Curtarolo, High-throughput electronic band structure calculations: Challenges and tools, Comput. Mater. Sci. **49**, 299 (2010).

[34] F. Hecht, New development in freefem $^{++}$, J. Numer. Math. **20**, 251 (2012).

[35] R. McPhedran, A. Movchan, and N. Movchan, Platonic crystals: Bloch bands, neutrality and defects, Mech. Mater. **41**, 356 (2009).

[36] S. Brand, R. A. Abram, and M. A. Kaliteevski, Complex photonic band structure and effective plasma frequency of a two-dimensional array of metal rods, Phys. Rev. B **75**, 035102 (2007).

[37] F. Lemoult, N. Kaina, M. Fink, and G. Lerosey, Wave propagation control at the deep subwavelength scale in metamaterials, Nat. Phys. **9**, 55 (2013).

[38] D. Röhlig, V. Laude, R. Zichner, F. Thieme, A. Thränhardt, and T. Blaudeck, Radio wave attenuation by a large-scale photonic crystal sculpture, Sci. Rep. **15**, 12317 (2025).

[39] V. Laude, Rigid cylinders in air, *Phononic Crystals* (De Gruyter, Berlin, München, Boston, 2015), Chap. 4.2.1, pp. 109–112.